Influence of premixed chlorine salt on the pore characteristics of cement-based hardened grout containing a large amount of bentonite

Xiaohong Niu [a,b,c], Guorui Feng [a,b,*], Yanna Han [a,b,*], Adam Bezuijen [c,d], Tingye Qi [a,b], Jinwen Bai [a,b]

[a] College of Mining Engineering, Taiyuan University of Technology, Taiyuan 030024, China

[b] Key Laboratory of Shanxi Province for Mine Rock Strata Control and Disaster Prevention, Taiyuan 030024, China

[c] Laboratory of Geotechnics, Ghent University, Technologiepark 68, Ghent 9052, Belgium

[d] Unit Geo-Engineering, Deltares, Delft, The Netherlands

ABSTRACT

Moderate content of premixed chlorine salt could improve the fluidity and strength of cement-based grouts containing a large amount of bentonite, while its effect on pore structure is still unclear. In this study, pore characteristics were systematically described by low-field NMR combined with low-pressure CO_2 and N_2 adsorption. Pores were classified into five types according to their size to clarify the effect of chloride content, curing time, and chloride type (NaCl or $CaCl_2$) on various pore volumes. This was further analyzed by the introduction of unit volume variation (U). Results show that the volume of inter gel pore (2–10 nm) and middle capillary pore (50–1000 nm) increases with the increase of chloride content while that of fine (10–50 nm) and large (> 1000 nm) capillary pore decreases. The inter gel pore volume and fine capillary pore volume depend on C–S–H content and surfactant micelles number, respectively. The volume of middle and large capillary pores is mainly affected by the hydration product content. For intra sheet pores (< 2 nm), their volumes show an inverted "N" shape with the increase of NaCl content and a "U" shape for $CaCl_2$, which is mainly related to the ettringite dissolution and nano-SiO_2 dispersion. The chloride content and curing time also have a large reduction effect on the U of intra sheet pores, fine and large capillary pores. Furthermore, $CaCl_2$ contributes more than NaCl to the development of pore structure, especially for inter gel pores and middle capillary pores.

Keywords: Cement-based grout mixed with bentonite; Low-field NMR; Pore structure; Chlorine salt

* Corresponding author at: College of Mining Engineering, Taiyuan University of Technology, Taiyuan, Shanxi 030024, China. E-mail address: fguorui@163.com (G. Feng), hanyanna0504@163.com (Y. Han).

1. Introduction

Bentonite is always used in clay-cement mixtures due to its great fluid properties and ability to prevent solids settling (bleeding), and also produces a low-permeability hardened material that is ideal for sealing groundwater inflow and strengthening surrounding rock of a deeply fractured rock mass [1]. Nevertheless, the large incorporation of bentonite (reaches about 50%) reduces the workability of fresh slurry due to the strong water absorption of montmorillonite, which is the main component of bentonite, and decreases the mechanical properties of hardened grout because of the reduction in cement content [2]. Thus, in our previous study, nano-SiO_2 (NS) and accelerator (chlorine salts such as NaCl and $CaCl_2$) were added to the material to improve the weakened mechanical properties [3]. Unexpectedly, it was found that not only the uniaxial compressive strength of the cement-based grout containing a large amount of bentonite was improved by the synergistic effect of surfactant (sodium dodecyl sulfate, SDS) and chlorine salt, but also the dispersion of NS and fluidity of fresh slurry were modified. Based on the composition analysis of products, the mechanical enhancement was initially attributed to the filling effect of well-dispersed NS and matrix compaction associated with the formation of calcium aluminosilicate hydrate (C–A–S–H) and Friedel's salt ($C_3A{\cdot}CaCl_2{\cdot}10H_2O$). The filling effect of Friedel's salt could refine the pore structure and improve the mechanical properties of hardened grout, but mainly enhance the early strength. Nevertheless, the pore structure evolution of hardened grouts has not been systematically analyzed. Moreover, grout is a highly disordered, multi-phase, and complex porous material consisting of micropores to macropores [4]. As a porous material, the microscopic properties of the pore system such as size distribution and connectivity play a significant role in determining macroscopic capacity in terms of permeability, strength, durability, and other mechanical properties and thus the suitability and effectiveness for engineering application [5, 6]. The effects of different pores on the macroscopic properties vary significantly. Specifically, gel pores will lead to the shrinkage and creep of grouts [7], whereas capillary pores will affect strength and durability [8]. Therefore, a further precise description and characterization of the pore system are essential for understanding the performance of the grout.

Chlorine salt, as one of the most widely used accelerators, was added to improve the performance of cement-based grouts containing a large amount of bentonite in our previous mixture design [3].

Chlorine salt can accelerate the hydration or reaction of the cement or supplementary cementitious materials and quickly enhance the early strength [9, 10]. The early strengthening effect is mainly attributed to the reaction between chloride ions and tricalcium aluminate (C_3A), which calls chloride binding and finally forms Friedel's salt [11]. When NaCl is introduced into the cement-based material, it will firstly react with $Ca(OH)_2$ and then react with C_3A, as shown in Eqs (1) and (2), respectively [12]. While for $CaCl_2$, it will directly react with C_3A shown in Eq. (2). Accelerators do improve early strength but understanding the effect of NaCl or $CaCl_2$ on the pore characteristics of hardened grouts is also equally essential. The microstructural evolution of materials affected by chloride has been reported in existing studies. Concretely, the reduction of porosity was found in cement paste with chlorides using a water saturation method, which was mainly attributed to the formation of Friedel's salt [13]. Conversely, the increased porosity was also reported through the mercury intrusion porosimetry (MIP) method after the addition of chlorine salt, which might be due to the Ca^{2+} leaching [14]. In the above studies, the pore structure of samples with and without chlorine salts was compared to analyze the influence of chlorides. However, some conflicting conclusions are obtained and the effect of chloride (e.g. content and type) on various pores is still unclear. In addition, the dispersion of NS was effectively improved under the synergistic effect of SDS and chlorine salt, which may further have some effects on the pore characteristics.

$$Ca(OH)_2 + 2NaCl = CaCl_2 + 2Na^+ + 2OH^- \tag{1}$$

$$C_3A + CaCl_2 + 10H_2O \rightarrow C_3A \cdot CaCl_2 \cdot 10H_2O \tag{2}$$

Methods used to study the pore characteristics of cement-based materials include low-pressure CO_2 adsorption, N_2 adsorption, MIP, low-field nuclear magnetic resonance (LF-NMR), scanning electron microscopy (SEM), etc. [4, 15]. The application scope of some methods is shown in Fig. 1 [16, 17]. It can be observed that MIP and LF-NMR cover a larger pore size range than other quantitative methods. The MIP has been widely used to evaluate the porosity and pore size distribution of cement pastes and concretes [18, 19]. However, it can only capture information about interconnected meso-/macropores and may result in artificial micro-cracks at capillary pressure over confining pressures. Compared with MIP, LF-NMR characterizes the pore structure of materials by detecting the hydrogen proton signal of pore water. Thus, LF-NMR can test both connected and non-connected pores and has

the greatest advantage of providing non-destructive and continuous detection [16]. Moreover, LF-NMR is capable of characterizing pore size from micro-scale to macro-scale and is suitable for the determination of gel and capillary pores, which makes it particularly convenient for achieving a comprehensive microstructure characterization of hardened grouts [20, 21]. Furthermore, as the most important hydration product in cement-based materials, calcium silicate hydrate (C–S–H) gel has many pores with a pore size distribution between 1 and 10 nm [7]. Among the above methods, the N_2 adsorption method tests micropores and sub-micropores, particularly in the range of 2–50 nm [22], while CO_2 adsorption tests micropores whose size is less than 2 nm. Thus, a combined measurement of low-pressure CO_2 and N_2 adsorption allows relatively full testing of nanoscale pores, which is expected to provide additional information on the pore structure of grout.

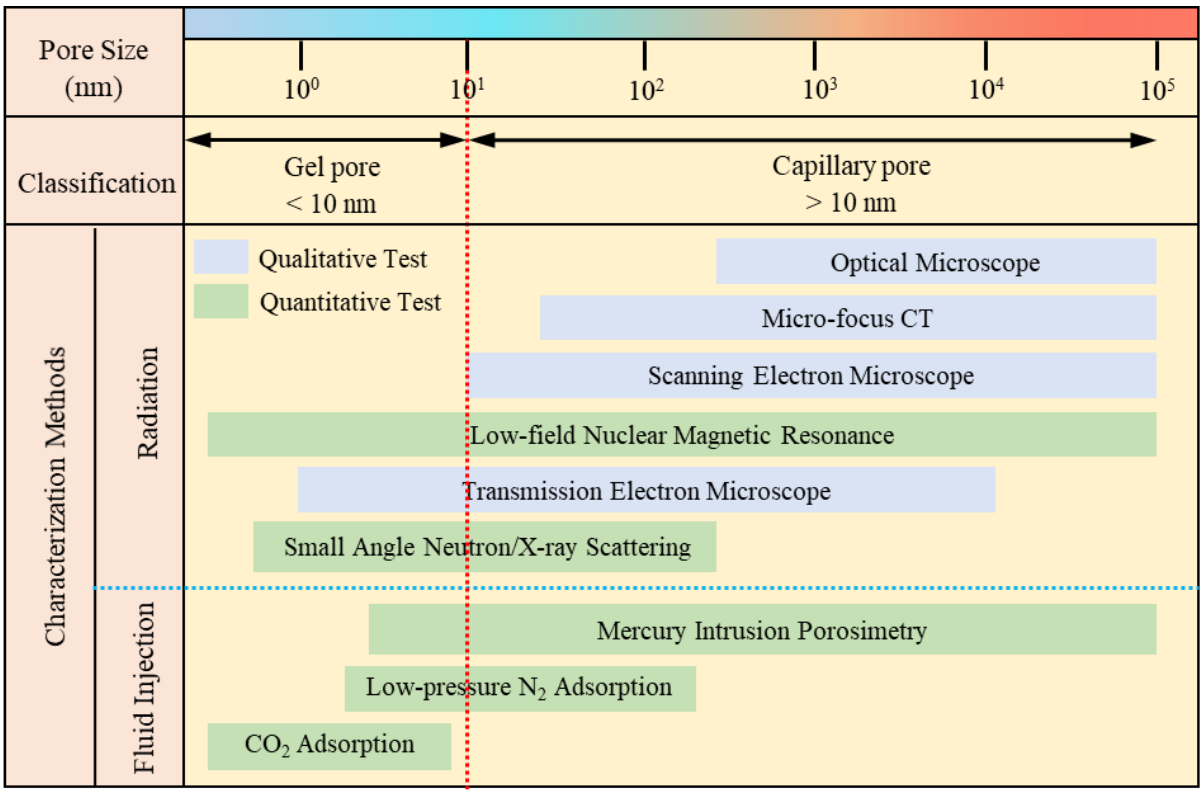

Fig. 1. Application scope of some pore structure test methods [16, 17].

In this paper, the pore structure of hardened grout was classified into two major categories (gel pores and capillary pores) with a pore size of 10 nm as the dividing line (as shown by the red dashed line in Fig.1). Five subcategories were further divided according to their pore size (intra sheet pores: < 2 nm, inter gel pores: 2–10 nm, fine capillary pores: 10–50 nm, middle capillary pores: 50–1000 nm, and large capillary pores: > 1000 nm). Then, the T_2 spectrum distribution of grouts cured at 28 days

was tested by LF-NMR, and the volumes of different pores were obtained by calculating the peak area. Low-pressure CO_2 and N_2 adsorption tests were also performed to obtain additional information on the pore structure. The volume variation and underlying mechanism of various pores with the chloride content and type (NaCl and $CaCl_2$) were further discussed. Furthermore, the pore structure of grouts cured at different times (3, 7, and 28 days) was also tested to explore the effect of chloride on various pores at different curing times. Finally, the effect of chloride on pore structure was further studied by introducing the unit volume variation (U), which represented the unit change of various pores volume with increasing chlorine content (U_c) or curing time (U_t).

2. Experimental

2.1 Sample preparation

The grout is composed of cement (PC), bentonite (Bt), NS suspension, naphthalene-based superplasticizer (FDN), water glass (WG), and water. The NS suspension is obtained by adding the SDS, chlorine salt (NaCl or $CaCl_2$), and NS to the water. A water/(PC + Bt) ratio of 1.2 is chosen for its popularity in grouting applications. The mass ratio of PC to Bt is considered to be 1.0. The NS content is 2%, which is the most used content to improve the performance of concrete. The mass ratio of SDS to NS is 0.05:1 and the contents of NaCl and $CaCl_2$ are shown in Table 1. The amount of FDN is 1%, within the recommended dosage of 0.5% to 1.0%. The 2% WG is chosen for its ability to shorten the setting time of fresh slurry and enhance the strength of hardened grouts. It is worth noting that the above materials are all in percentage of the total mass of PC and Bt. Moreover, grout without any chlorides is also prepared to further clarify the effect of chloride on the pore structure.

The prepared fresh slurry is shaped in a cylindrical mold with a diameter of 50 mm and a height of 100 mm. Then the samples are cured at an ambient temperature of 20 ± 2 °C and relative humidity of 95% for three different times (3, 7, and 28 days). The samples cured for 28 days are further divided into two groups (group A and B) according to the added chloride type, as shown in Table 1. To facilitate the analysis of subsequent results, the grouts are named as AB-X, where A represents the percentage content of chlorine salt, B is the chloride type, and X is the curing time. The sample without any chlorides in the control group is designated as 0-28. After the samples are cured to a predetermined time, LF-NMR tests, low-pressure CO_2 and N_2 adsorption experiments are performed sequentially.

Due to the limitations of test conditions, the number of samples in each test condition is one. Thus, in order to reduce the effect of non-uniformity on the test results, the uniformity of samples is improved by extending the stirring time and using a concrete vibrating table to vibrate the fresh grout during the casting process. A schematic diagram of the preparation process and tests of grouts is shown in Fig. 2.

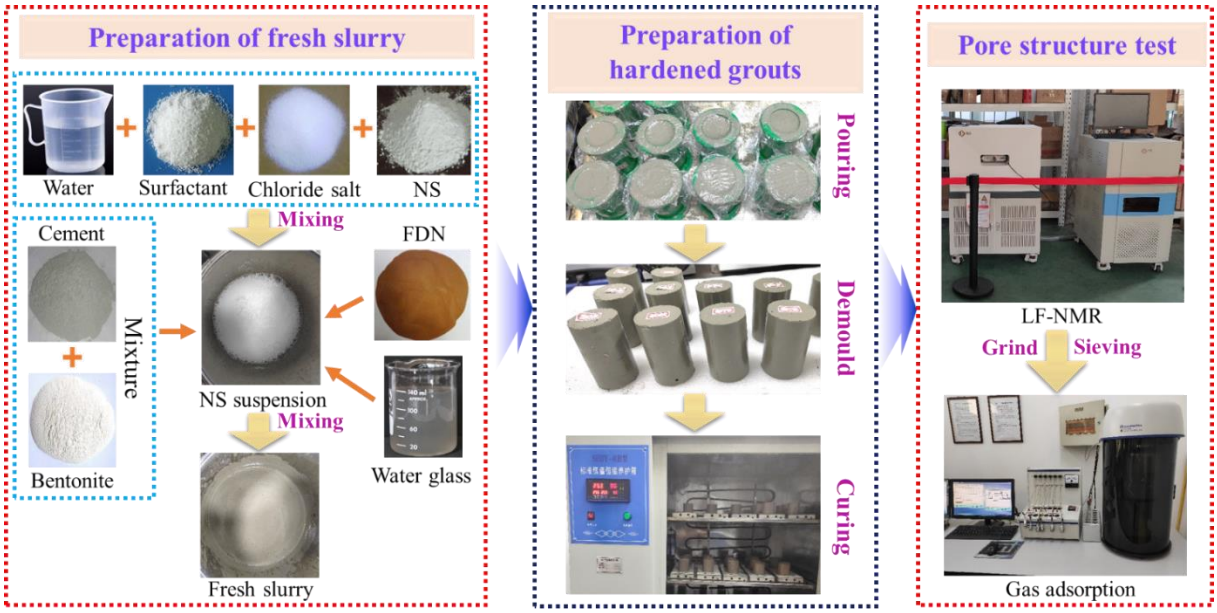

Fig. 2. Schematic diagram of grout fabrication and test process.

Table 1

Mixture design of grouts.

Group	Chloride type	Chloride content (%)	Curing time (days)	Sample ID
–	–	0	28	0-28
A	NaCl	0.5	28	0.5Na-28
		1.0		1.0Na-28
		1.5		1.5Na-28
		2.0		2.0Na-28
		2.5		2.5Na-28
B	$CaCl_2$	0.10	28	0.10Ca-28
		0.25		0.25Ca-28
		0.50		0.50Ca-28
		0.75		0.75Ca-28

		1.00		1.00Ca-28
–	NaCl	1.5	3	1.5Na-3
–			7	1.5Na-7
–	$CaCl_2$	0.50	3	0.50Ca-3
–			7	0.50Ca-7

2.2 Methods

2.2.1 Classification of pores

The range of pore sizes in the cement pastes spans many orders of magnitude, which can be classified into two major categories: gel pores formed by the C–S–H gel and capillary pores formed by the mixed water that is not involved in the hydration reaction [21]. The gel pores contain intra C–S–H sheet pores and inter C–S–H particle gel pores, with sizes of 0.5–1.8 nm and 2–10 nm, respectively [23, 24]. Capillary pores can also be further divided into fine, middle, and large pores. Thus, five subcategories of pores are identified in this study according to the following pore size: intra sheet pores (< 2 nm), inter gel pores (2–10 nm), fine capillary pores (10–50 nm), middle capillary pores (50–1000 nm) and large capillary pores (> 1000 nm) [25, 26]. It should be noted that some micropores in the grouts are also classified as intra sheet pores.

2.2.2 LF-NMR measurement

Pore characteristics of the sample can be depicted by the LF-NMR signal (amplitude, peak area, and continuity) of the transverse relaxation time (T_2) spectrum and pore size can be transformed from T_2 according to Eq. (3) [27, 28]. Before the LF-NMR test, cylindrical hardened grouts are firstly vacuum-saturated with distilled water for 24 h. To eliminate the influence of water evaporation on the results, grouts are wiped with wet paper towels after being removed from distilled water and wrapped with sealing tape. Then the LF-NMR experiments are conducted using a MacroMR12-150H-I spectrometer (Suzhou Niumag Analytical Instrument Co., Ltd., China) with a constant magnetic field strength of 0.3 T and a resonance frequency of 12.98 MHz. The magnetic uniformity is as low as 30 ppm, and relaxation from gas diffusion could be ignored. A Carr-Purcell-Meiboom-Gill (CPMG) sequence is used to measure T_2. The echo spacing, wait time, number of echoes, number of scans, and test temperature are 0.2 ms, 3000 ms, 8000, 64, and 35 °C, respectively.

$$\frac{1}{T_2} \approx \frac{1}{T_{2,surf}} = \rho_2 \left(\frac{S}{V} \right) = F_s \times \frac{\rho_2}{r} \tag{3}$$

where T_2 is the transversal relaxation time of water in the pores; $T_{2,surf}$ is the transversal relaxation time due to surface relaxation; S/V is specific surface area; F_s is a geometrical factor, equalling to 2.0 for cylindrical pores; ρ_2 is surface relaxivity; r is pore radius. Normally, surface relaxivity relates to the "thickness" of the surface layer, which is regarded as 50 μm/s in this study according to [29].

2.2.3 Low-pressure CO_2 and N_2 adsorption

The low-pressure CO_2 adsorption experiments and low-pressure N_2 adsorption experiments are conducted using a physical adsorption instrument (TriStar 3020 II) to reflect the information related to intra sheet pores and fine capillary pores, respectively. The grouts are crushed (60–80 mesh) and degassed after fully drying. CO_2 adsorption experiments are performed under a relative pressure (P/P_0) ranging from 0 to 0.03 at 273.15 K. The intra sheet pore volume is interpreted using Brunauer-Emmett-Teller (BET) model. N_2 adsorption experiments are conducted at a constant liquid nitrogen temperature of 77 K with P/P_0 ranging from 0.01 to 0.99. The fine capillary pore volume is obtained from the N_2 adsorption-desorption data based on the Barrett-Joyner-Halenda (BJH) model.

3. Results and Discussion

3.1 Effect of chloride content on pore structure

3.1.1 LF-NMR analysis

The relaxation properties for the fully saturated hardened grouts are shown in Fig. 3. The left figure shows the LF-NMR T_2 spectrum, where the upper axis is the pore radius converted by Eq. (3). The right figure presents the cumulative LF-NMR signal. It could be found that the grouts cured for 28 days show a multimodal distribution, illustrating the irregularity and complexity of the pore structure. LF-NMR signals of the grout are mainly distributed in three regions, from left to right, representing the inter gel pores, middle capillary pores, and large capillary pores, respectively. The strongest T_2 peak appears in 1–10 ms and occupies a majority of the total LF-NMR signal, indicating that middle capillary pores are the main component of pore structure. As chloride content increases, the first and second peaks and cumulative LF-NMR signal increase continuously, while the peaks associated with large capillary pores are decreased. After adding NaCl or $CaCl_2$, the pore structure

evolution of grouts with the chloride content is similar, but there are some differences in specific quantitative indicators.

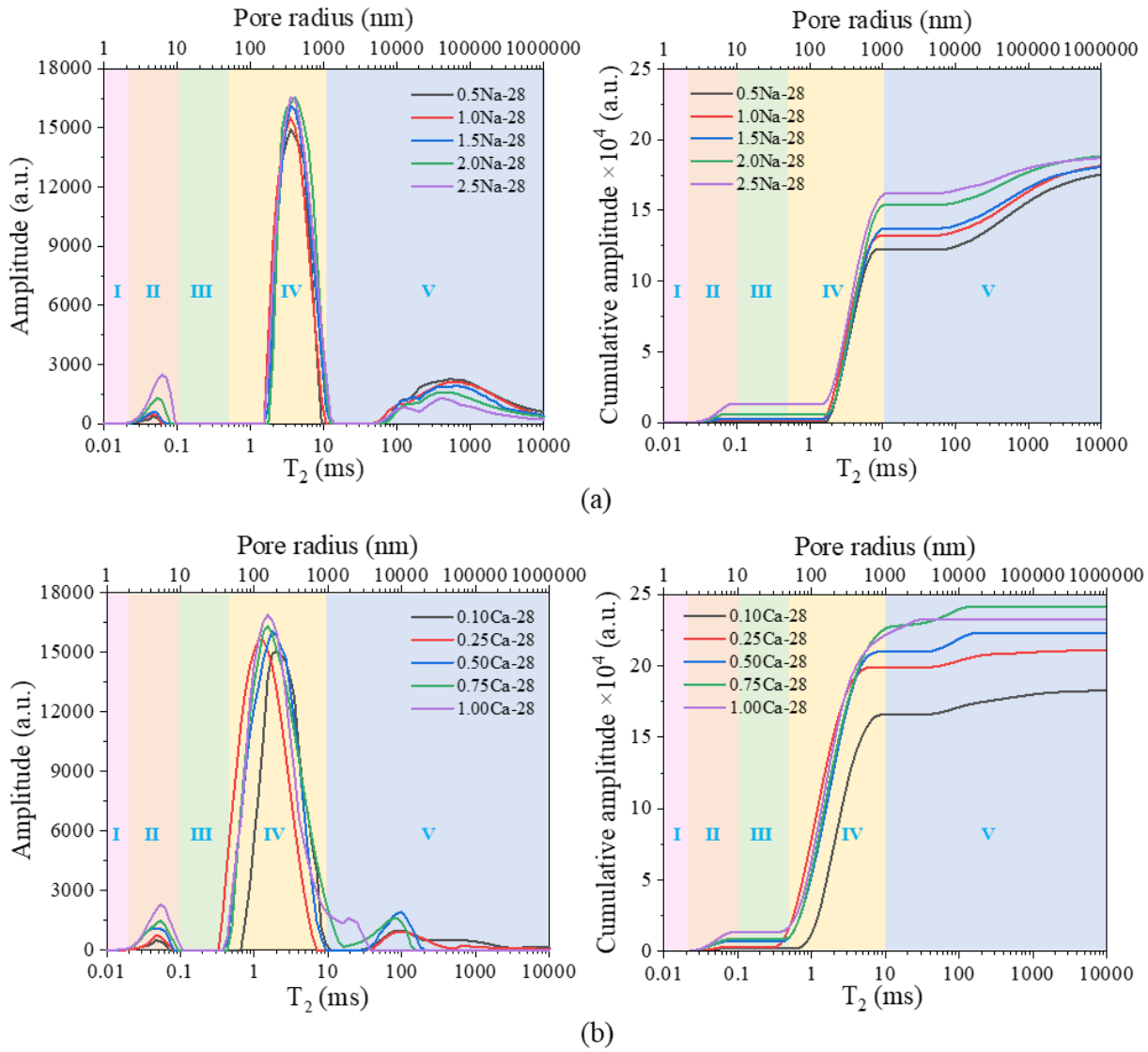

Fig. 3. LF-NMR T_2 distributions of grouts in groups A (a) and B (b), (Ⅰ: intra sheet pore, Ⅱ: inter gel pore, Ⅲ: fine capillary pore, Ⅳ: middle capillary pore, and Ⅴ: large capillary pore).

Four peaks could be identified from the LF-NMR T_2 spectrum of grouts in group A (Fig. 3a). The first peak is mainly distributed at the range of 0.02–0.09 ms, representing the inter gel pores. The second peak locates between 1.5 and 14 ms, corresponding to a pore size of 150–1400 nm, which means that the majority of the second peak is in the middle capillary pores range, with a small proportion being large capillary pores. The third and fourth peaks are connected and distributed between 50 and 10000 ms (5000–1000000 nm), illustrating that the two peaks represent large capillary pores. The connection between T_2 peaks is an index defining the connectivity of pore size, and the

valley with no signal presents non-connection [30]. Thus the connection between the third and fourth peaks indicates the continuity in the size distribution of large capillary pores. A constant shift of the first and second peaks to the right could also be observed, indicating that an increase in NaCl content will make the smaller pores (such as inter gel pores and middle capillary pores) transform to larger sizes. Different from the above peaks, no clear monotonic left or right shift is observed on the two right peaks. The LF-NMR T_2 spectrum suggests trimodality for grouts in group B (Fig. 3b). The second peak lies between 0.33 and 16 ms (33–1600 nm), meaning that most of the second peak represents middle capillary pores and a small part is fine capillary pores and large capillary pores. The connection between the second and third peaks could be observed to be strongly affected by the $CaCl_2$ content, changing from non-connected at low content to connected at high levels. The rightward shift of the first peak is also noticed, but not on the second peak, suggesting that the increase of $CaCl_2$ content does not lead to a shift of middle capillary pores toward the larger pore size. Conversely, the third peak undergoes a leftward shift, implying a transition of large capillary pores from large sizes to small sizes.

To further understand the effect of chlorine salt content on the pore characteristics, the T_2 distribution of samples before and after adding chloride is compared, and the results are shown in Fig. 4. For the grouts added with chloride, samples 0.5Na-28 and 0.10Ca-28 are purposely selected for comparison, as they have the lowest total LF-NMR signal in each group. It can be found that the total LF-NMR signal of sample 0-28 in the control group is still lower than those in the test group, elucidating that the incorporation of chlorine salt could increase the pore volume. The first and second peaks of the grout without chloride are lower than those with chloride. It can also be noticed that the T_2 peaks associated with middle and large capillary pores shift to the right after the incorporation of NaCl or $CaCl_2$, which suggests that chlorine salt could lead to the shift of capillary pores toward large size.

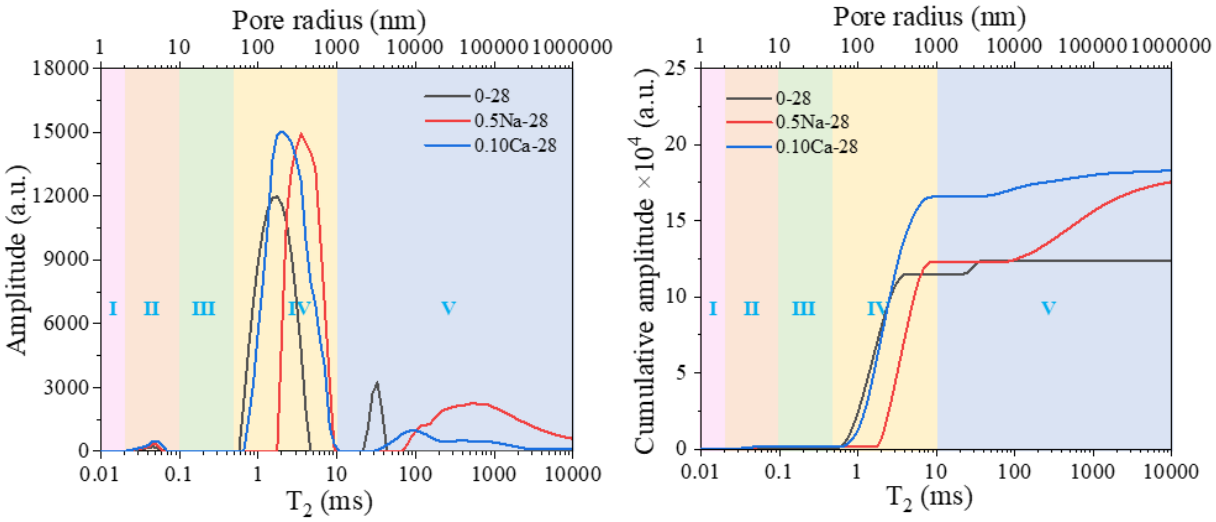

Fig. 4. LF-NMR T_2 distribution of grouts with and without chloride.

It does not seem to be a reliable method to use the peak height of the T_2 spectrum to judge the pore volume of grouts. Because the widths of T_2 peaks are inconsistent and the direct comparison of peak heights is prone to errors, leading to its usage only for preliminary, qualitative, and simple analysis. In this context, the area under the T_2 spectrum, representing the total signal of H atoms in the sample [16], is calculated to quantify the pore volume. It is worth noting that the area of each peak could be obtained directly from the test results. However, as can be observed in Fig. 3, a peak sometimes spans more than one pore type, so the volumes of different pores are recalculated according to their pore size and the results are shown in Fig. 5. It should be noted that the volume fractions of intra sheet pores and fine capillary pores are not shown in the figure, although they are included in the total area, which will be systematically analyzed in Sections 3.1.2 and 3.1.3.

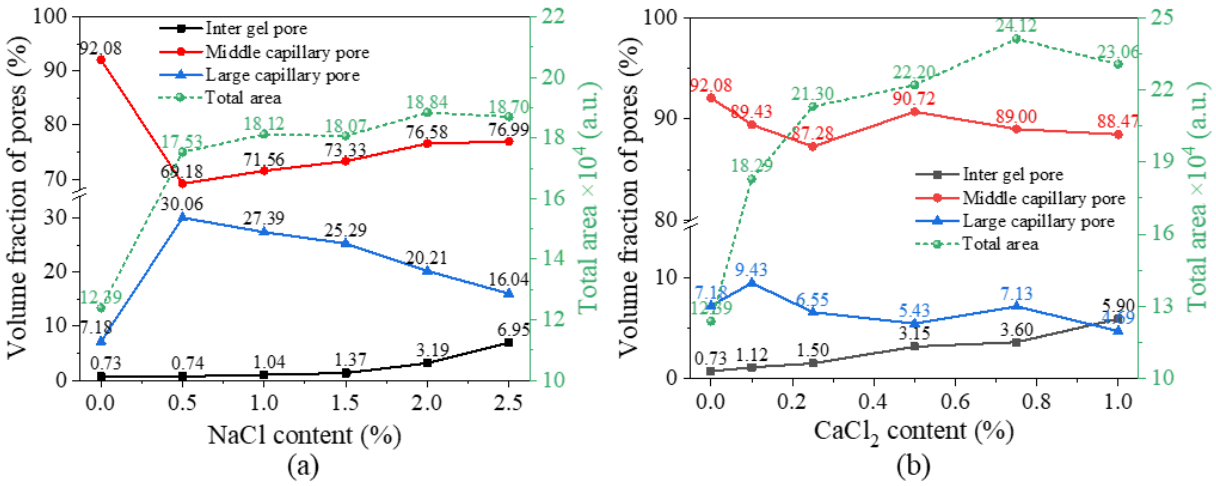

Fig. 5. Total T_2 spectrum area and pore volume fraction of grouts in groups A (a) and B (b).

As can be seen in Fig. 5, the pore structure of all hardened grouts is dominated by middle capillary

pores, followed by large capillary pores, and least by inter gel pores, which is consistent with the report [31]. The total pore volume (i.e., the total area shown in Fig. 5) of the grout with chloride is significantly higher than that without chloride, with a maximum growth rate of 52.06% for NaCl (2.0Na-28) and 94.67% for $CaCl_2$ (0.75Ca-28). The significant increase in porosity is mainly attributed to the effect of salt on the void ratio of bentonite, and partly to the ettringite dissolution and Ca^{2+} leaching from the hardened grout [32]. It has been reported that the bentonite saturated with salt solution has a larger void ratio than that of the bentonite saturated with distilled water under the same suction [33]. During the preparation of fresh slurry, a mixture of cement and bentonite is firstly added to the NS suspension, which contains a large amount of chlorine salts, and then the admixtures are added. Since the slurry has good fluidity, it can be assumed that the bentonite is in a saturated state in the fresh slurry. In addition, the shaped samples are cured in the same humidity (95%), thus the suction environment of the hardened grouts could be regarded as the same. Therefore, the high void ratio of bentonite further contributes to the higher porosity of hardened grout with chloride than that without chloride. The thermodynamic stability conditions of ettringite can be affected by pH, and its dissolution increases with the increase of pH [34]. When chloride is added to the cement system, Cl^- is adsorbed by C–S–H or participates in some chemical reactions, so that cation (Na^+ or Ca^{2+}) becomes free. To balance the charge, the cation will be bound into OH^-, resulting in an increased pH and finally aggravating ettringite dissolution. The Ca^{2+} leaching may also be responsible for the increased total pore volume, which could be accelerated by chloride ions [32]. The vacuum-saturation of the sample before the LF-NMR test provides conditions for Ca^{2+} leaching. The inter gel pores, deriving from C–S–H gels, also show a higher volume fraction in grouts containing chloride. The highest inter gel pore volume fractions of grouts in groups A and B are 9.52 times and 8.08 times higher than that in the control group. The increased volume fraction may be related to the role of chlorine salt on the promotion of C_3A and tricalcium silicate (C_3S) hydration and then more C–S–H gels are formed [10]. The incorporation of chloride reduces the volume fraction of middle capillary pores, and the reduction effect of NaCl is more pronounced than $CaCl_2$. It can also be observed that the volume fraction of middle capillary pores tends to increase with the increase of chloride content, and if the content continues to increase, the same volume fraction as the control group (92.08%) may be reached.

However, according to our previous test results, when the NaCl content increased from 0.5% to 2.5% or $CaCl_2$ content increased from 0.10% to 1.00%, the uniaxial compressive strength of the hardened grouts showed a tendency to decrease, especially for the 28-day strength [3]. Following this variation in mechanical properties, the strength may continue to decline if the chloride content is further increased, which may eventually result in the grout losing its application value. Thus, the maximum content of NaCl and $CaCl_2$ in this study is 2.5% and 1.00%, respectively. For large capillary pores, the addition of NaCl increases their volume, which may still be associated with the high void ratio of bentonite under the salt solution, ettringite dissolution and Ca^{2+} leaching. $CaCl_2$ could also lead to an increase in the volume fraction of large capillary pores. However, when the $CaCl_2$ content continues to increase, the volume fraction keeps decreasing and is lower than that in the control group (7.18%), where the filling effect of Friedel's salt needs to be responsible.

A different volume variation of pores is observed with the change of chloride content. The total pore volume increases with the increase of chloride content. However, when the chlorine salt content is the highest, such as 2.5Na-28 and 1.00Ca-28, the total pore volume decreases slightly, which is probably due to the constant content of cement in the grouts having the maximum chloride binding capacity [35, 36]. The volume fractions of inter gel pores and middle capillary pores increase as the chloride increases, while that of large capillary pores is decreasing. Large fluctuations in the volume fraction of capillary pores can also be found, especially in the middle capillary pores of grouts in group B. It has been reported that fully hydrated cement pastes typically contain about 23% non-evaporable water [16]. Actually, the mixed water is much greater than this value and the redundant water undergoes different degrees of evaporation leading to the generation of capillary pores. As a result, the volume of capillary pores fluctuates slightly. The decrease of large capillary pores may correspond to some interactions between grout constituents. Firstly, when chlorides are internally mixed in cement-based materials, the cement hydration is accelerated, leading to more precipitation of C–S–H [37]. The higher the chloride content, the stronger the promotion of cement hydration, and the more obvious the decrease in pore volume. Secondly, the observed decrease can be partially attributed to the precipitation of Friedel's salt. It is commonly recognized that voluminous chloride-bearing compounds, such as Friedel's salt, preferentially precipitate in the coarser pores [38]. Besides, according to [39], the

morphology of Friedel's salt is a hexagonal slice with a size of 2–3 μm, which is within the size range of large capillary pores. The higher the chloride ion concentration, the more opportunities for chloride ions to enter the binding site [35, 36], leading to more formation of Friedel's salt. Preferential growth of products in larger spaces is also responsible for the increase in the volume fraction of middle capillary pores. A large number of new pores are formed that are smaller than the original size, where the middle capillary pores dominate. This means that the original large capillary pores are divided and filled by Friedel's salt and other hydration products, leading to the increase of middle capillary pores. The increase in gel pore volume fraction is related to the massive formation of C–S–H gels. Theoretically, the total pore volume should decrease with the increase of chloride content due to the filling effect of formed Friedel's salt and C–S–H gels. However, an opposite experimental result is obtained. This may be mainly due to the higher void ratio of the bentonite, because bentonite will have a relatively higher porosity when it is saturated at a higher salt concentration [33]. Therefore, under the influence of large amount of bentonite, the total pore volume of hardened grout increases with the increase of chloride content. The increasing pore volume may also be partly related to the ettringite dissolution and Ca^{2+} leaching. In addition, it can also be seen that the total T_2 spectrum area of samples in group B is significantly greater than that in group A, while the large capillary pore volume is lower. $CaCl_2$ also has a stronger contribution to the increase in inter gel pore volume than NaCl, because a small gradient change in the $CaCl_2$ content could result in a larger variation in the volume fraction. The underlying mechanism of pores influenced by the chloride type will be further discussed in Section 3.3.

3.1.2 Intra sheet pores analysis

LF-NMR is indeed an effective method for non-destructively quantifying the pore structure of concrete [4]. However, the T_2 value for the water chemically bound to the C–S–H gel is too short to be fully detected by the CMPG sequence [16, 40]. For the test of supermicropores (pore diameter < 2 nm), a better solution is to use CO_2, whose molecular diameter is about 0.33 nm, as the probe gas to obtain more pore information [41]. Thus the intra sheet pores are detected by the low-pressure CO_2 adsorption test to make up for the flaw of LF-NMR and the results are shown in Figs. 6 and 7.

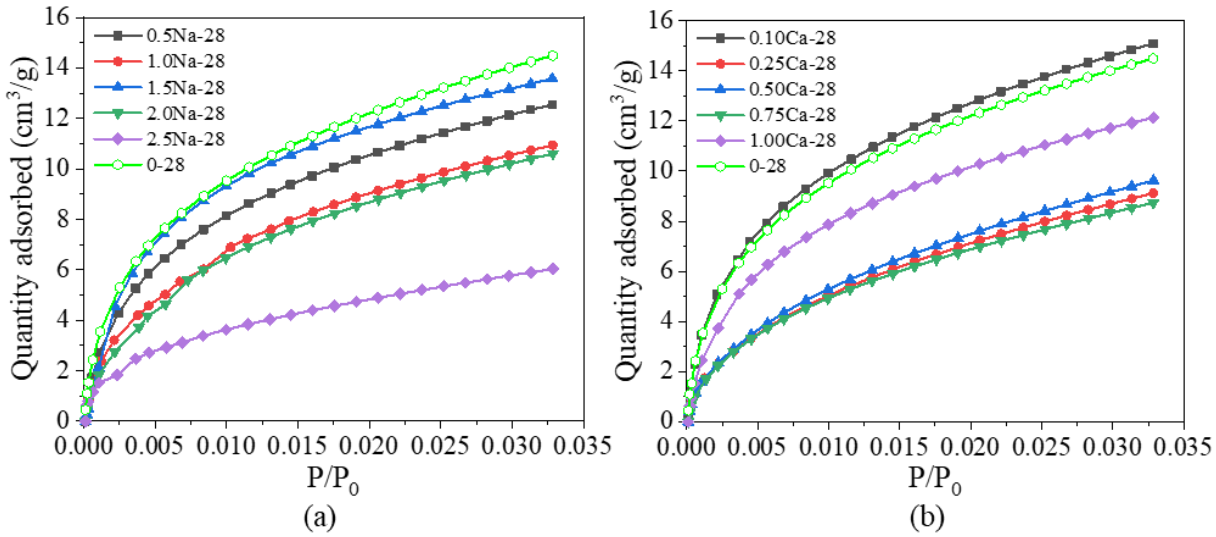

Fig. 6. CO_2 adsorption isotherms of hardened grouts in groups A (a) and B (b).

It can be seen that for all hardened grouts, the adsorbed amount of CO_2 increases rapidly, and then the increased rate gradually slows down with the increase of P/P_0. According to the International Union of Pure and Applied Chemistry (IUPAC) classification, the CO_2 adsorption isotherms belong to Type I, indicating the existence of micropores (< 2 nm). The adsorbed CO_2 volume (i.e., intra sheet pore volume) of sample 0-28 is higher than other grouts, except for the sample 0.10Ca-28, which may be caused by the lower NS dispersion in the grouts [3]. The lower dispersion means that NS is prone to agglomerate, which will make NS lose part of the filling effect on micropores and further lead to an increase in intra sheet pore (micropore) volume.

The intra sheet pore volume decreases with the increase of NaCl content and then increases and finally decreases again, showing an inverted "N" shape. The decrease of intra sheet pore volume at lower NaCl content may be due to the adsorption of Cl^- by hydration products. It is well accepted that Cl^- can be adsorbed by the chemical adsorption layer and microcrystalline lattice in the C–S–H, which increases C–S–H chain length and degree of polymerization [42] and further contribute to a decrease in the intra sheet pore volume. Dissolution of ettringite may be responsible for the subsequent increase of intra sheet pore volume. The increased NaCl content raises the pH of system, which intensifies the dissolution of ettringite. The final decrease may be related to the improvement of NS dispersion. It has been reported in our previous study that increasing the NaCl content could significantly improve the NS dispersion [3], which may further reduce the intra sheet pore volume due to the filling effect of NS. In group B, the intra sheet pore volume shows an overall trend of first decreasing and then increasing

with the increase of $CaCl_2$ content, which looks like a "U" shape, and no further decrease is observed. Although sample 0.50Ca-28 has a slightly higher pore volume than 0.25Ca-28 and 0.75Ca-28, the difference is small compared to the variation of other volumes. Thus, the small increase can be considered as fluctuation and neglected. The absence of the second decrease is due to the well-dispersed NS in all five levels of $CaCl_2$ content used in this study [3]. The above analysis regarding the intra sheet pores further indicates that low-pressure CO_2 adsorption tests can compensate for the limitations of LF-NMR in the characterization of the pore structure of C–S–H gels.

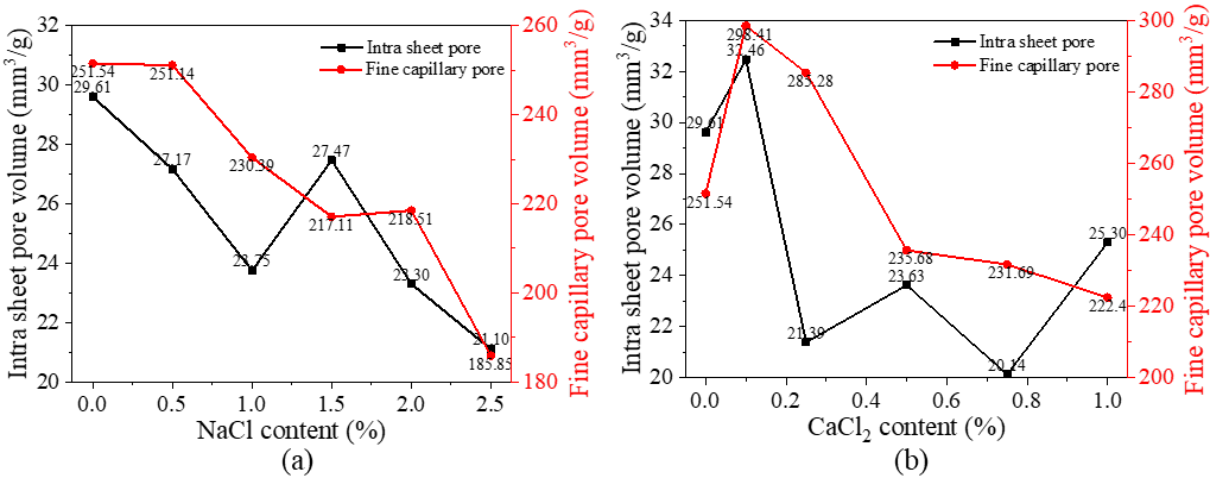

Fig. 7. The volume of intra sheet pores and fine capillary pores of grouts in groups A (a) and B (b).

3.1.3 Fine capillary pores analysis

To clarify the effect of chlorine salt on fine capillary pores, a volume analysis of pore diameters smaller than 50 nm is attempted using a low-pressure N_2 adsorption device, which can measure the pore size between 2 and 50 nm [22]. According to the pore classification in this study, both inter gel pores and fine capillary pores will be tested. Thus, the pore volume with a size of 10–50 nm is recalculated and presented in Fig. 7.

The volume of fine capillary pores of sample 0-28 is higher than that of samples in group A, which may be related to the filling effect of SDS micelles in the grouts containing chloride. The formation of SDS micelles under the synergistic effect of SDS and chlorine salt has been reported in our previous study [3]. The characteristic length of surfactant micelle is about 20 nm [43], which lies in the size range of fine capillary pores (10-50 nm) and thus can act as a filler. In group B, the fine capillary pore volume is higher than that in the control group when $CaCl_2$ content is low, which is probably associated with the filling effect of Friedel's salt on large capillary pores, the same as the

reason for the increase in the middle capillary pore volume. The absence of the phenomenon that the pore volume of grouts in group A higher than that in sample 0-28 is because $CaCl_2$ could lead to more formation of Friedel's salt than NaCl [3]. The SDS micelles do, of course, play a filling effect, which may not compensate for the volume increase caused by the filling effect of the generated Friedel's salt. When $CaCl_2$ content is high, the lower pore volume of grouts with $CaCl_2$ than that without any chlorides is perhaps still attributed to the filling effect of SDS micelles.

The fine capillary pore volume decreases continuously with the increase of chloride content. It is recognized that the increase of chloride content will increase the aggregation number of ionic micelles [43], which is beneficial to the filling effect of SDS micelles and the reduction of the fine capillary pore volume. It can be found that the reduction effect of $CaCl_2$ is higher than that of NaCl, because the increase rate of 0.9% $CaCl_2$ content causes a reduction in the pore volume of 76.01 mm^3/g, while that of 2.0% NaCl is 65.29 mm^3/g. The underlying mechanism will be further analyzed in Section 3.3. In addition, it can also be seen that the fine capillary pore volume in the grouts is significantly higher than the intra sheet pore volume, while the signal related to fine capillary pores cannot be detected in most of the samples during the LF-NMR test. The possible reason is that the sample is not fully saturated and there are no H atoms in some of the non-connected pores, which do not contain free water absorbed during the saturation process or adsorbed water generated during the hydration reaction. The foregoing analysis further indicates that the low-pressure N_2 adsorption could provide additional pore information on grouts.

3.2 Effect of chloride on pore structure at different curing times

3.2.1 LF-NMR analysis

Grouts containing the most moderate content of chloride (1.5% NaCl or 0.50% $CaCl_2$) from the five levels used in this study are selected and cured at different times to further study the effect of chloride on the pore characteristics and the results are shown in Figs. 8 and 9. At the early stage (3 days), the pore structure of grout with 1.5% NaCl is mainly composed of middle and large capillary pores, while at the later time the middle capillary pores become the main component. For grout containing 0.5% $CaCl_2$, the pore structure mainly consists of middle capillary pores, followed by large capillary pores, which is hardly influenced by the curing time. The T_2 peak representing the middle

capillary pores shifts to the left with curing time, implying that pores have been refined due to the various chemical reactions within components. The connectivity of T_2 spectra has changed, gradually shifting from connected at 3 days to non-connected at 28 days, which may be attributed to the filling effect of hydration products in some larger pores. It can also be found that the total pore volume and volume fraction of inter gel pores and middle capillary pores increase with curing time, while that of large capillary pores decreases. The reduction of large capillary pores can be understood from the following. As the cement hydration progresses, a large number of hydration products, such as C–S–H and ettringite, are generated. In addition, the incorporation of chlorine salts (Na^+, Ca^{2+}, and Cl^-) promotes the hydration of cement, which leads to the formation of more C–S–H gels. Secondly, the observed decrease can be partially attributed to the precipitation of Friedel's salt. Finally, the reduction is also expected to be partly due to the formation of C–A–S–H gels. It is accepted that Al^{3+} present in bentonite can promote the polymerization of C–S–H gels into C–A–S–H gels [44]. Our previous research also found that the C–A–S–H content increased with curing time [3]. The mean chain length of C–A–S–H is about 28.3, which is larger than that of C–S–H (7.5), resulting in a larger particle size than C–S–H [45]. Thus, the effect of C–A–S–H on reducing the volume is stronger than C–S–H. The above reasons should also be responsible for the increase in middle capillary pore volume, as discussed in Section 3.1.1. The increase in the inter gel pore volume is mainly related to the increasing C–S–H content with curing time. In addition, the reduction in the volume fraction of large capillary pores by 0.5% $CaCl_2$ is 20.7% from 3 to 28 days, while that by 1.5% NaCl is 26.51%, which is not a significant difference between them. The increments in inter gel pore volume fraction by NaCl and $CaCl_2$ are 0.69% and 1.43%, respectively. The above phenomena indicate that the low content of $CaCl_2$ could almost reach or even exceed the effect of high NaCl content on the variation of pore volume, which will be thoroughly discussed in Section 3.3.

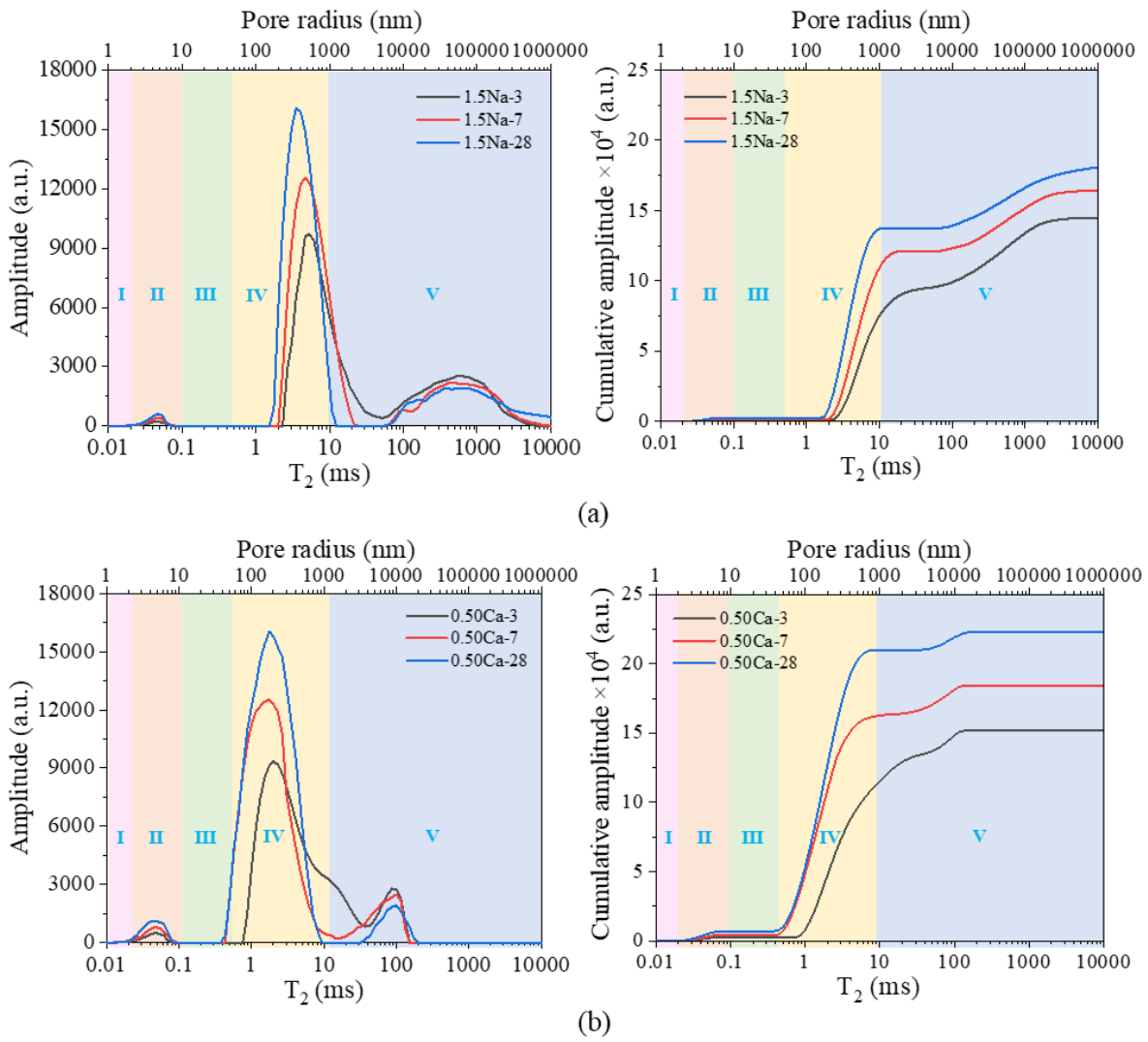

Fig. 8. LF-NMR T_2 distributions of hardened grouts with 1.5% NaCl (a) or 0.50% $CaCl_2$ (b) cured at different times.

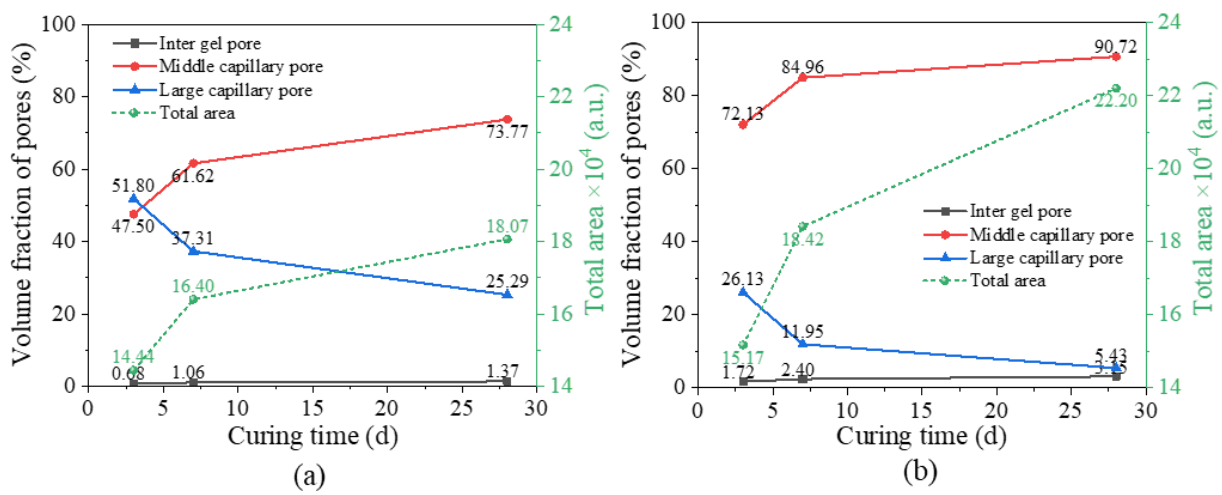

Fig. 9. Total T_2 spectrum area and pore volume fraction of grouts with 1.5% NaCl (a) or 0.50% $CaCl_2$ (b) cured at different times.

3.2.2 Intra sheet pores analysis

The information concerning the intra sheet pores is shown in Figs. 10 and 11. According to the IUPAC classification, the CO_2 adsorption isotherms belong to Type I, which are not affected by the curing time. It can be found that the adsorbed CO_2 amount, i.e. intra sheet pore volume increases with curing time, which can be understood from four aspects. Firstly, as the cement hydration proceeds, the C–S–H gel, which is generated in large quantities, is mainly responsible. The increasing amount of amorphous C–S–H gel changes the pore structure and increases the gel pore volume [46]. Secondly, the crystalline linkage of hydration products is partially responsible for the increase, which will convert large pores into smaller pores (micropores) [47]. Thirdly, the hydration reaction of cement consumes the residual water in grouts, which may lead to the generation of some micropores. Lastly, the increase is also associated with the evaporation of some physically adsorbed water in the gel pores during the curing process.

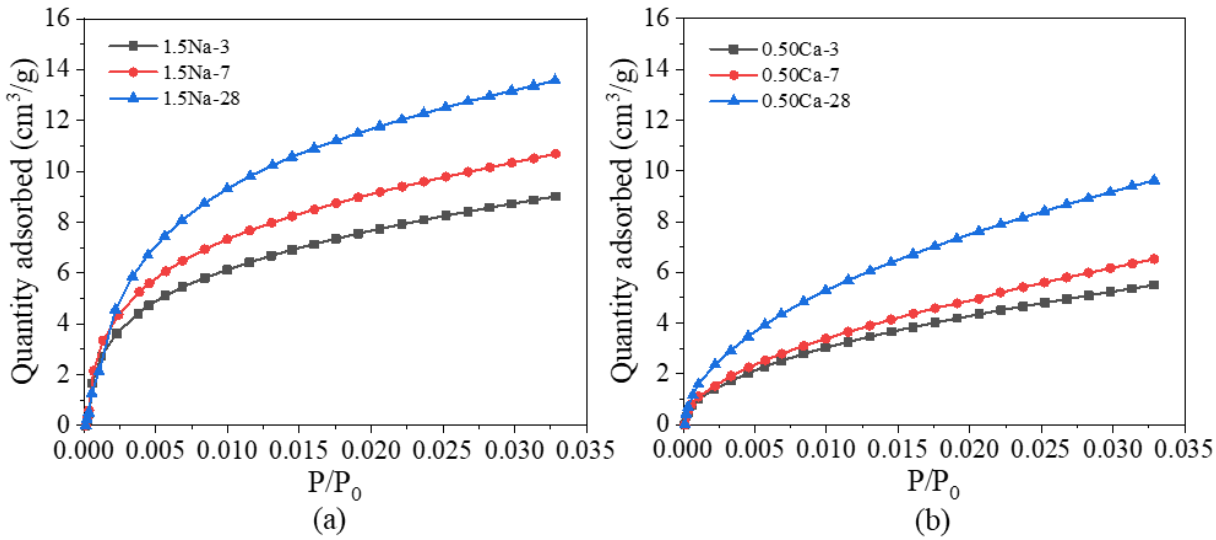

Fig. 10. CO_2 adsorption isotherms of grouts with 1.5% NaCl (a) or 0.50% $CaCl_2$ (b) cured at different times.

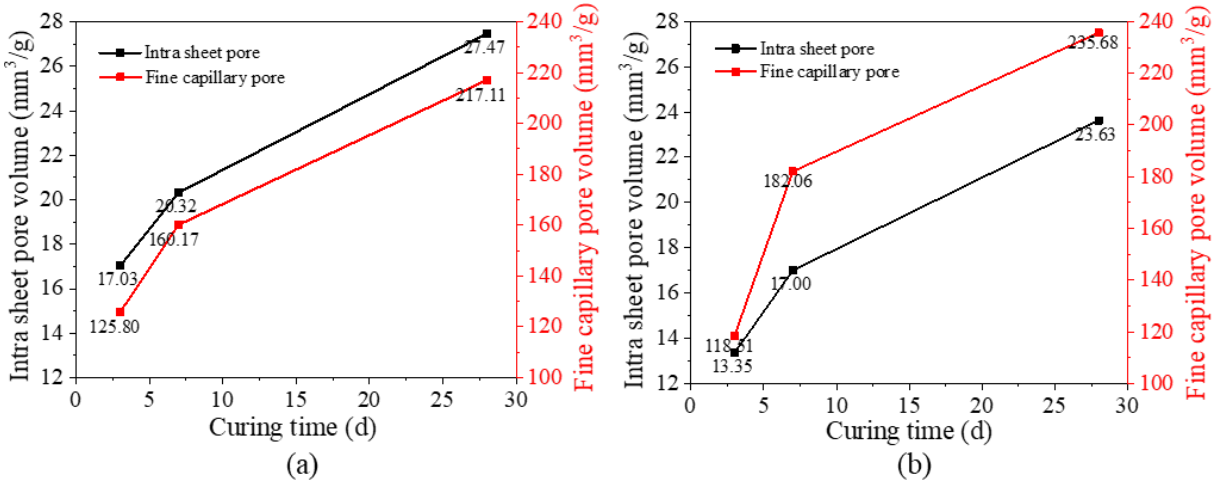

Fig. 11. The volume of intra sheet pores and fine capillary pores of grouts cured at different times.

3.2.3 Fine capillary pores analysis

The recalculated fine capillary pore volumes are shown in Fig. 11. It can be seen that the volume of fine capillary pores increases with curing time. On the one hand, with the progress of cement hydration, the pores are gradually filled with hydrates such as C–S–H, C–A–S–H, ettringite, Friedel's salt, and others, which leads to the transformation of pores from large to small size and eventually increases the fine capillary pore volume. On the other hand, this phenomenon may be related to the shrinkage of grouts. The main mechanism for the development of shrinkage in hydrated cement paste is the removal of water held by hydrostatic tension in fine capillary pores and the loss of physically adsorbed water in the C–S–H gels. Autogenous shrinkage will occur as water held in capillary pores is consumed during the cement hydration process, which often occurs in capillary pores with a size smaller than 50 nm [48].

3.3 Effect of chloride type on pore structure

Based on the mixture design in Table 1, grouts with identical content of NaCl or $CaCl_2$ (taking 0.5% as a representative content) are compared to understand the effect of chloride type on pore structure and the results are shown in Fig. 12. It can be seen that T_2 peaks associated with middle and large capillary pores of sample 0.50Ca-28 are located at the left of sample 0.5Na-28, indicating that $CaCl_2$ will lead to a finer middle and large capillary pore size. The total LF-NMR signal of 0.50Ca-28 (22.20×10^4) is also significantly higher than that of 0.5Na-28 (17.53×10^4), which may be due to the higher void ratio of the bentonite in sample 0.50Ca-28. This is because the bentonite prepared with $CaCl_2$ solution has a larger void ratio compared to the bentonite prepared with NaCl [49]. The high

signal of 0.50Ca-28 may also be related to the leaching of Ca^{2+} because the leaching caused by $CaCl_2$ is larger than that of NaCl due to its higher diffusion coefficient and concentration of Cl^- [50]. Furthermore, the dissolution of ettringite should also be responsible, since the higher charge of divalent Ca^{2+} than Na^+ will require more OH^- to balance the charge, leading to a higher pH that eventually accelerates the ettringite dissolution. These mentioned above can also be used to understand the higher total T_2 spectrum area of group A samples than group B samples (Fig. 5), as mentioned in Section 3.1.1. It can also be observed that $CaCl_2$ results in higher inter gel pore volume and middle capillary pore volume than NaCl. The high inter gel pore volume may be associated with the higher content of generated C–S–H. It has been reported that $CaCl_2$ has a more significant accelerating effect on C_3S hydration than NaCl [51], which generates more C–S–H. Furthermore, due to the high hydration-promoting effect of $CaCl_2$, the inter gel pore volume of grout with 0.50% $CaCl_2$ in each curing time is higher than that with 1.5% NaCl at the same curing time, as shown in Fig. 9. The high middle capillary pore volume should be attributed to the filling effect of Friedel's salt. In our previous study, we found that $CaCl_2$ could result in more Friedel's salt formation than NaCl [3]. The filling of large capillary pores with Friedel's salt leads to the generation of smaller pores, which increases the volume of middle capillary pores. Distinct from inter gel pore and middle capillary pore, the large capillary pore volume fraction of 0.50Ca-28 (5.43%) is significantly smaller than that of 0.5Na-28 (30.06%), which is primarily attributed to the filling effect of Friedel's salt. Secondly, the formation of a large amount of C–S–H by $CaCl_2$ is also responsible, which could also play a filling effect. The greater production of C–S–H gels and Friedel's salt caused by $CaCl_2$ further explains the lower volume fraction of large capillary pores in grout with 0.5% $CaCl_2$ than that with 1.5% NaCl (Fig. 9) at the same curing time.

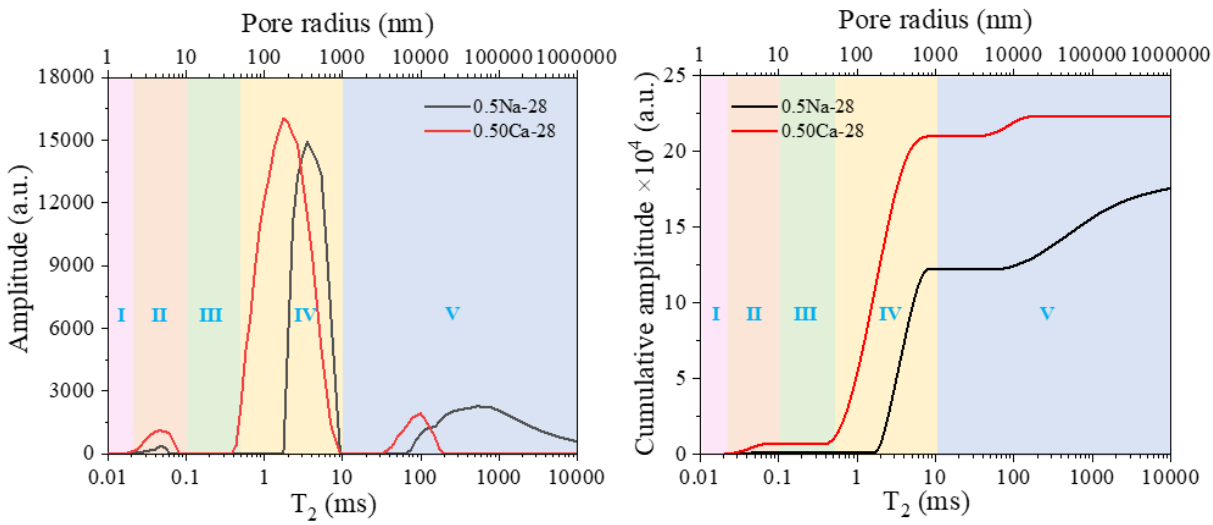

Fig. 12. LF-NMR T_2 distributions of hardened grouts with 0.5% chlorine salt.

Comparing the adsorbed CO_2 amount in Fig. 6 and intra sheet pore volume in Fig. 7, it can be found that sample 0.5Na-28 has a larger intra sheet pore volume than 0.50Ca-28, which may be related to the lower NS dispersion of grout with 0.5% NaCl. The evaporation of water from NS agglomerates could lead to the formation of some micropores. According to our previous study, NS precipitation was observed at the vial bottom when the NaCl content was 0.5%, while this phenomenon was not observed in the NS suspension with $CaCl_2$ [3]. The higher improvement of NS dispersion by $CaCl_2$ than NaCl also helps to understand the underlying mechanism that the intra sheet pore volume of grout with 1.5% NaCl is higher at each curing time than that with 0.50% $CaCl_2$ at the same age, as illustrated in Fig. 11.

It could also be found from Fig. 7 that 0.5% $CaCl_2$ leads to a lower fine capillary pore volume than 0.50% NaCl, which is related to the effect of cation on SDS micelles. $CaCl_2$ has a greater promotion effect on SDS micelle generation than NaCl [43]. On the one hand, the presence of chloride drives the micelles toward larger sizes, especially in the presence of excess chlorides. The effect is less prominent for NaCl, which is perhaps not surprising since Ca^{2+} is a divalent ion and thus the ionic strength of the solution is increased relative to NaCl. On the other hand, the introduction of $CaCl_2$ drives the SDS to form more compact micelles with a smoother surface, while the micelles appear disordered and fluctuate in shape in the presence of Na^+. Both of the above-mentioned points contribute to the filling effect of SDS micelles in the fine capillary pores, which also further explains the high reduction effect of $CaCl_2$ on the fine capillary pore volume than NaCl, as described in Section 3.1.3.

3.4 Effect of chloride on unit pore volume variation

Unit volume variation (U), meaning the unit change of various pores volume with increasing chloride content (U_c) or curing time (U_t), is introduced in this paper to further understand the effect of chloride on pore structure, which is calculated according to Eqs (4) and (5), respectively.

$$U_c = \frac{V}{C} \tag{4}$$

$$U_t = \frac{V}{T} \tag{5}$$

where U_c represents the unit variation of pore volume with chloride content; U_t means the unit change of pore volume with curing time; V is the pore volume; C is the percentage content of chlorine salts; T represents the curing time of hardened grout.

Fig. 13 shows the U_c of grouts in groups A and B. It can be seen that with the increase of NaCl or $CaCl_2$ content, the U_c regarding intra sheet pore, fine, middle, and large capillary pores decreases, indicating that the change (increase or decrease) in pore volume is not linearly correlated with the change rate of chloride content. The U_c associated with inter gel pores shows a decreasing and then increasing variation. The initial decrease may be due to the generation of C–A–S–H by polymerization of most C–S–H gels, which decreases the increased rate of inter gel pore volume. The subsequent increase of U_c is related to the promotion of C–S–H production by chlorine salts. Since the content of Al^{3+} in the system is certain, it will limit the polymerization process of C–S–H, although the process is still going on. In group A, the increase of NaCl content has the greatest effect on the U_c regarding the large capillary pores, followed by intra sheet pores and fine capillary pores, and the lowest influence on middle capillary pores. The high reduction of U_c associated with intra sheet pores, fine and large capillary pores is related to the limited NS content, SDS content, and chloride binding sites in the grouts, respectively [37]. In group B, the U_c of intra sheet pores and fine capillary pores is greatly affected by the $CaCl_2$ content, while the inter gel pores are least affected. Comparing the U_c in the two groups, it can be found that the reduction rate of U_c regarding intra sheet pores, fine, middle and large capillary pores of grouts in group B is significantly higher than that in group A, which is directly attributed to the higher promotion effect of $CaCl_2$ than NaCl on the dispersion of NS and the generation of SDS micelles, C–S–H and Friedel's salt.

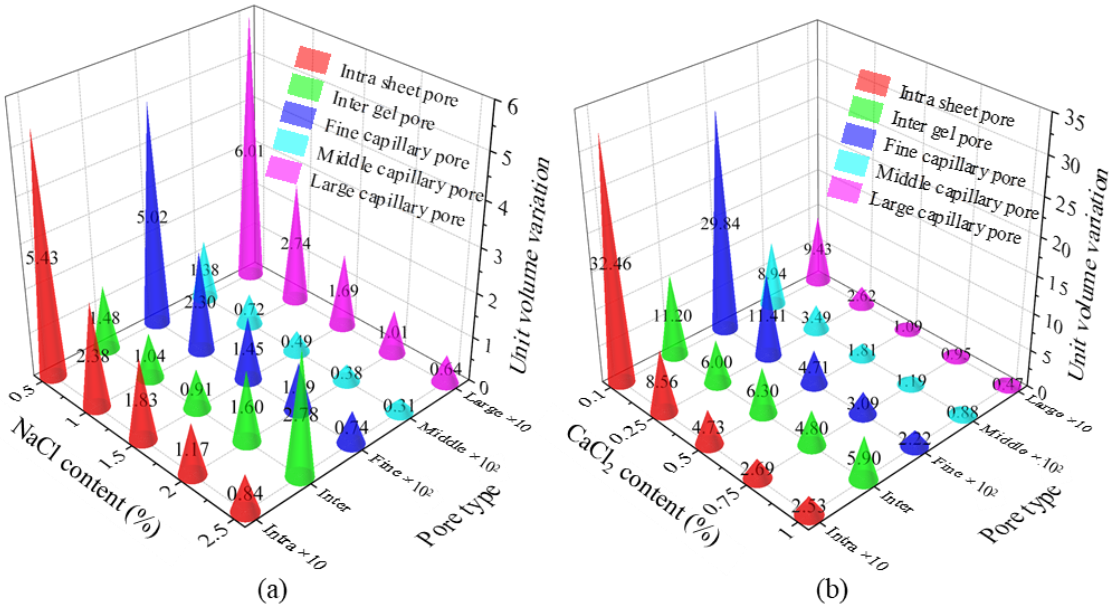

Fig. 13. U_c of grouts in groups A (a) and B (b).

The U_t of grouts with 1.5% NaCl or 0.50% $CaCl_2$ is presented in Fig. 14. It can be found that the U_t of five types of pores decreases with the increase of curing time, meaning that the change rate of pore volume is relatively large at the early curing time and decreases slowly at the later stages. For grout with NaCl, the greatest reduction in U_t is associated with large capillary pores, followed by intra sheet pores and fine capillary pores, and the smallest for the middle capillary pores. It can be seen from Fig. 14(b) that curing time has the greatest effect on U_t of large capillary pores, followed by inter gel pores and intra sheet pores, and the least effect is on the middle capillary pores. The strong reduction in U_t of the large capillary pores during the early stages is related to the faster hydration of cement-based materials at these early stages, resulting in the formation of a large number of products that can play a filling role, which further leads to a reduction in the U_t of fine capillary pore. As the curing time increases, the amount of free and bound water consumed by hydration and evaporation gradually decreases, which could reduce the U_t of intra sheet pores and fine capillary pores. A large amount of C–S–H is generated in the early stage of hydration, thus the U_t of inter gel pores is large. In the later stage, although some C–S–H is still generated, the content is relatively small and the U_t of inter gel pores decreases. The higher U_t associated with inter gel pores in grout with $CaCl_2$ than that with NaCl further verifies the higher promotion of C–S–H production by $CaCl_2$.

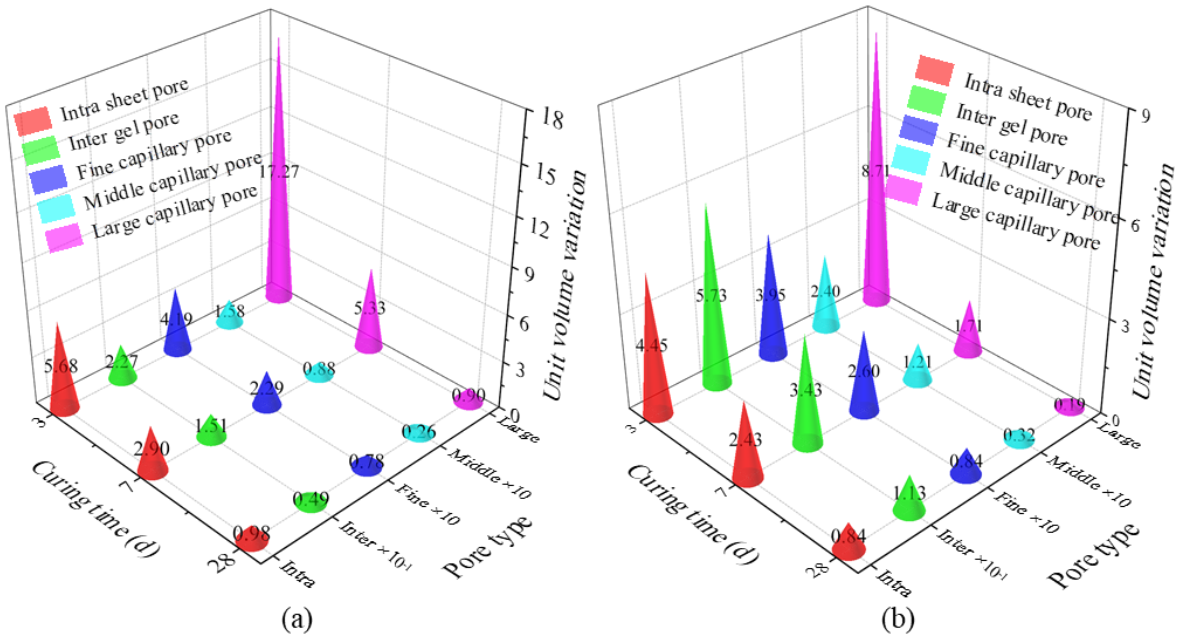

Fig. 14. U_t of grouts with 1.5% NaCl (a) or 0.50% $CaCl_2$ (b).

4. Conclusions

In this paper, low-field NMR combined with low-pressure CO_2 and N_2 adsorption tests is conducted to analyze the effect of chloride content, curing time, and chloride type on the volume of various pores in the cement-based hardened grouts containing a large amount of bentonite. The main conclusions are summarized as follows:

(1) Incorporation of chlorine salt increases the total pore volume of hardened grouts, with a maximum increase rate of 52.06% for NaCl and 94.67% for $CaCl_2$, which is mainly due to the increased void ratio of bentonite under the salt solution. Chloride also has a great influence on the volume of various pores. Specifically, chloride increases the volume of inter gel pores and middle capillary pores, while decreasing the fine and large capillary pore volume. This increasing or decreasing trend is continuously magnified with the increase of chloride content. Different from the above four pore types, the volume of intra sheet pores presents an inverted "N" shape with the increase of NaCl content and shows a "U" shape for $CaCl_2$. The unit volume variation of inter gel pores first decreases and then increases with the increase of chloride content, while that of other pores decreases.

(2) The effect of mixture design on the volume of various pores is governed by different factors. Intra sheet pores, including some micropores, are mainly associated with ettringite dissolution and nano-SiO_2 dispersion. The inter gel pores, which mainly derive from the C–S–H gels, undoubtedly

depend on the C–S–H content. The volume of fine capillary pores is mainly dependent on the number and size of SDS micelles in the NS suspension and partly related to the filling effect of hydration products on larger pores. For middle and large capillary pores, their volume is mainly affected by the hydration product content, such as C–S–H, C–A–S–H, ettringite, and Friedel's salt.

(3) Curing time will affect the connectivity of pore size distribution, changing from connected at an early age to non-connected at a later age. As curing time increases, the volume fraction of large capillary pores decreases continuously due to the filling effect of generated products, while the volume of other pores increases. The variation of intra sheet pore volume with curing time is mainly related to the amount and crystalline linkage of hydration products, and the consumption and evaporation of water in the grouts. The fine capillary pore volume is associated with the generated product amount and the shrinkage degree of hardened grouts. Curing time will greatly reduce the unit volume variation of large capillary pores, while the reduction effect on other pores is relatively small.

(4) $CaCl_2$ is more conducive to the development of pore structure, as the total LF-NMR signal of grout with $CaCl_2$ is significantly higher than that with the same content of NaCl. $CaCl_2$ could also lead to a higher inter gel pore volume and middle capillary volume due to the higher promotion of $CaCl_2$ on cement hydration and Friedel's salt production, which further results in a smaller large capillary pore volume. The volumes of intra sheet pores and fine capillary pores of grout with $CaCl_2$ are lower than those with NaCl owing to the better dispersion of NS and higher promotion of SDS micelle production by $CaCl_2$, respectively.

There is a tight connection between the pore structure and the macroscopic properties of grouts. In this paper, a quantitative and systematic analysis of pore characteristics is carried out using three different methods. However, the relationship between pore structure and macroscopic properties of grouts has not been established. It should therefore be emphasized that extra work is essential to better understand the relationship between various pores and macroscopic properties of hardened grouts in terms of permeability and strength.

Acknowledgements

This work was financially supported by Distinguished Youth Funds of National Natural Science Foundation of China (No. 51925402), and Shanxi Science and Technology Major Project (No.

20201102004). X.H. Niu is also grateful for the financial support from the Chinese Scholarship Council (No. 202106930012) towards her joint PhD at Ghent University, Belgium. The authors are very grateful to the editors and reviewers for their kind and invaluable comments.

References

[1] J. Zhang, L. Liu, F. Zhang, J. Cao, Development and application of new composite grouting material for sealing groundwater inflow and reinforcing wall rock in deep mine, Sci. Rep. 8 (2018) 5642. https://doi.org/10.1038/s41598-018-23995-y.

[2] J. Liu, X. Gong, X. He, R. Zhang, R. Li, Experimental study of mortar samples containing sodium bentonite, J. Test. Eval. 48 (2020) 3579–3587. https://doi.org/10.1520/JTE20170324.

[3] X. Niu, G. Feng, Y. Han, Q. Liu, G. Xue, J. Cui, C. Song, Synergistic effect of surfactant and chlorine salt on dispersion of nano-SiO_2 and performance of cement-based grout containing a large amount of bentonite, Cem. Concr. Compos. 131 (2022) 104587. https://doi.org/10.1016/j.cemconcomp.2022.104587.

[4] J. Hu, Q. Ren, D. Yang, S. Ma, J. Shang, X. Ding, Z. Luo, Cross-scale characteristics of backfill material using NMR and fractal theory, T. Nonferr. Metal. Soc. 30 (2020) 1347–1363. https://doi.org/10.1016/S1003-6326(20)65301-8.

[5] B. Park, Y.C. Choi, Hydration and pore-structure characteristics of high-volume fly ash cement pastes, Constr. Build. Mater. 278 (2021) 122390. https://doi.org/10.1016/j.conbuildmat.2021.122390.

[6] D. Jiao, C. Shi, Q. Yuan, X. An, Y. Liu, H. Li, Effect of constituents on rheological properties of fresh concrete-A review, Cem. Concr. Compos. 83 (2017) 146–159. https://doi.org/10.1016/j.cemconcomp.2017.07.016.

[7] J. Wang, S. Dong, C. Zhou, A. Ashour, B. Han, Investigating pore structure of nano-engineered concrete with low-field nuclear magnetic resonance, J. Mater. Sci. 56 (2021) 243–259. https://doi.org/10.1007/s10853-020-05268-0.

[8] S.W.M. Supit, F.U.A. Shaikh, Durability properties of high volume fly ash concrete containing nano-silica, Mater. Struct. 48 (2015) 2431–2445. https://doi.org/10.1617/s11527-014-0329-0.

[9] X. Dai, Q. Ren, S. Aydın, M.Y. Yardımcı, K. Lesage, G.D. Schutter, Enhancing thixotropy and structural build-up of alkali-activated slag/fly ash pastes with nano clay, Mater. Struct. 54 (2021) 163. https://doi.org/10.1617/s11527-021-01760-4.

[10] H. Li, C. Xu, B. Dong, Q. Chen, L. Gu, X. Yang, W. Wang, Differences between their influences of TEA and TEA·HCl on the properties of cement paste, Constr. Build. Mater. 239 (2020) 117797. https://doi.org/10.1016/j.conbuildmat.2019.117797.

[11] R. Talero, L. Trusilewicz, A. Delgado, C. Pedrajas, R. Lannegrand, V. Rahhal, R. Mejía, S. Delvasto, F.A. Ramírez, Comparative and semi-quantitative XRD analysis of Friedel's salt originating from pozzolan and Portland cement, Constr. Build. Mater. 25 (2011) 2370–2380. https://doi.org/10.1016/j.conbuildmat.2010.11.037.

[12] M. Ben-Yair, The effect of chlorides on concrete in hot and arid regions, Cem. Concr. Res. 4 (1974) 405–416. https://doi.org/10.1016/0008-8846(74)90106-9.

[13] C. Shi, X. Hu, X. Wang, Z. Wu, G.D. Schutter, Effects of chloride ion binding on microstructure

of cement pastes, J. Mater. Civil Eng. 29 (2017) 04016183. https://doi.org/10.1061/(ASCE)MT.1943-5533.0001707.

[14] B. Díaz, L. Freire, P. Merino, X.R. Nóvoa, M.C. Pérez, Impedance spectroscopy study of saturated mortar samples, Electrochimi. Acta, 53 (2008) 7549–7555. https://doi.org/10.1016/j.electacta.2007.10.042.

[15] X. Niu, Y. Han, G. Feng, J. Cui, Effect of the physicochemical structure of mudstone on readsorption behavior of water, Energy Fuel. 35 (2021) 386–396. https://doi.org/10.1021/acs.energyfuels.0c03101.

[16] L. Liu, Z. He, X. Cai, S. Fu, Application of low-field NMR to the pore structure of concrete, Appl. Magn. Reson. 52 (2021) 15–31. https://doi.org/10.1007/s00723-020-01229-7.

[17] Y. Zhao, B. Lin, T. Liu, Y. Zheng, Y. Sun, G. Zhang, Q. Li, Multifractal analysis of coal pore structure based on NMR experiment: A new method for predicting T_2 cutoff value, Fuel, 283 (2021) 119338. https://doi.org/10.1016/j.fuel.2020.119338.

[18] A. Dixit, H. Du, J. Dang, S.D. Pang, Quaternary blended limestone-calcined clay cement concrete incorporating fly ash, Cem. Concr. Compos. 123 (2021) 104174. https://doi.org/10.1016/j.cemconcomp.2021.104174.

[19] X. Han, B. Wang, J. Feng, Relationship between fractal feature and compressive strength of concrete based on MIP, Constr. Build. Mater. 322 (2022) 126504. https://doi.org/10.1016/j.conbuildmat.2022.126504.

[20] Y. Zhao, C. Wang, L. Ning, H. Zhao, J. Bi, Pore and fracture development in coal under stress conditions based on nuclear magnetic resonance and fractal theory, Fuel, 309 (2022) 122112. https://doi.org/10.1016/j.fuel.2021.122112.

[21] H. Zhao, X. Qin, J. Liu, L. Zhou, Q. Tian, P. Wang, Pore structure characterization of early-age cement pastes blended with high-volume fly ash, Constr. Build. Mater. 189 (2018) 934–946. https://doi.org/10.1016/j.conbuildmat.2018.09.023.

[22] Y. Wang, Q. Yuan, D. Deng, T. Ye, L. Fang, Measuring the pore structure of cement asphalt mortar by nuclear magnetic resonance, Constr. Build. Mater. 137 (2017) 450–458. https://doi.org/10.1016/j.conbuildmat.2017.01.109.

[23] A. Bede, A. Scurtu, I. Ardelean, NMR relaxation of molecules confined inside the cement paste pores under partially saturated conditions, Cem. Concr. Res. 89 (2016) 56–62. https://doi.org/10.1016/j.cemconres.2016.07.012.

[24] K. Liu, X. Cheng, C. Zhang, X. Gao, J. Zhuang, X. Guo, Evolution of pore structure of oil well cement slurry in suspension–solid transition stage, Constr. Build. Mater. 214 (2019) 382–398. https://doi.org/10.1016/j.conbuildmat.2019.04.075.

[25] W. Li, C. Long, V.W.Y. Tam, C.S. Poon, W. Duan, Effects of nano-particles on failure process and microstructural properties of recycled aggregate concrete, Constr. Build. Mater. 142 (2017) 42–50. https://doi.org/10.1016/j.conbuildmat.2017.03.051.

[26] Q. Zeng, K. Li, T. Fen-chong, P. Dangla, Pore structure characterization of cement pastes blended with high-volume fly-ash, Cem. Concr. Res. 42 (2012) 194–204. https://doi.org/10.1016/j.cemconres.2011.09.012.

[27] J. Zhao, H. Xu, D. Tang, J.P. Mathews, S. Li, S. Tao, Coal seam porosity and fracture heterogeneity of macrolithotypes in the Hancheng Block, eastern margin, Ordos Basin, China, Int. J. Coal Geol.

159 (2016) 18–29. https://doi.org/10.1016/j.coal.2016.03.019.

[28] H. Zhou, Q. Zhang, C. Dai, Y. Li, W. Lv, Y. Wu, R. Cheng, M. Zhao, Experimental investigation of spontaneous imbibition process of nanofluid in ultralow permeable reservoir with nuclear magnetic resonance, Chem. Eng. Sci. 201 (2019) 212–221. https://doi.org/10.1016/j.ces.2019.02.036.

[29] X. Hu, C. Shi, Q. Yuan, J. Zhang, G.D. Schutter, Changes of pore structure and chloride content in cement pastes after pore solution expression, Cem. Concr. Compos. 106 (2020) 103465. https://doi.org/10.1016/j.cemconcomp.2019.103465.

[30] D. Xue, Y. Liu, J. Zhou, X. Sun, Visualization of helium-water flow in tight coal by the low-field NMR imaging: An experimental observation, J. Petrol. Sci. Eng. 188 (2020) 106862. https://doi.org/10.1016/j.petrol.2019.106862.

[31] J. Chen, Y. Li, H. Zhou, Y. Li, H. Guo, Nuclear magnetic resonance study on concrete pore structure evolution under different curing environments, Advances in Characterization of Functional Composite Materials 74 (2022) 1819–1827. https://doi.org/10.1007/s11837-022-05221-3.

[32] Y. Wang, T. Ueda, F. Gong, D. Zhang, Meso-scale mechanical deterioration of mortar due to sodium chloride attack, Cem. Concr. Compos. 96 (2019) 163–173. https://doi.org/10.1016/j.cemconcomp.2018.11.021.

[33] Y. He, W. Ye, Y. Chen, K. Zhang, D. Wu, Effects of NaCl solution on the swelling and shrinkage behavior of compacted bentonite under one-dimensional conditions. Bull. Eng. Geol. Environ. 79 (2020) 399–410. https://doi.org/10.1007/s10064-019-01568-1.

[34] J. Qian, J. Yu, H. Sun, Y. Ma, Formation and function of ettringite in cement hydrates, J. Chinese Ceram. Soc. 45 (2017) 1569–1581. https://doi.org/10.14062/j.issn.0454-5648.2017.11.04.

[35] Q. Yuan, C. Shi, G.D. Schutter, K. Audenaert, D. Deng, Chloride binding of cement-based materials subjected to external chloride environment – A review, Constr. Build. Mater. 23 (2009) 1–13. https://doi.org/10.1016/j.conbuildmat.2008.02.004.

[36] C. Qiao, P. Suraneni, J. Weiss, Damage in cement pastes exposed to NaCl solutions, Constr. Build. Mater. 171 (2018) 120–127. https://doi.org/10.1016/j.conbuildmat.2018.03.123.

[37] S.E. Chidiac, D.K. Panesar, H. Zibara, The effect of short duration NaCl exposure on the surface pore structure of concrete containing GGBFS, Mater. Struct. 45 (2012) 1245–1258. https://doi.org/10.1617/s11527-012-9831-4.

[38] A.K. Suryavanshi, R.N. Swamy, Influence of penetrating chlorides on the pore structure of structural concrete, Cement concrete aggr. 20 (1998) 169–179. https://doi.org/10.1520/CCA10451J.

[39] R. Luo, Y. Cai, C. Wang, X. Huang, Study of chloride binding and diffusion in GGBS concrete, Cem. Concr. Res. 33 (2003) 1–7. https://doi.org/10.1016/S0008-8846(02)00712-3.

[40] J. Hu, Q. Ren, Q. Jiang, Y. Jiang, J. Shang, Z. Luo, Macroscopic and microscopic trans-scale characteristics of pore structure of mine grouting materials, T. Nonferr. Metal. Soc. 29 (2019) 1067–1081. https://doi.org/10.1016/S10036326(19)65015-6.

[41] S. Chen, S. Tao, D. Tang, H. Xu, S. Li, J. Zhao, Q. Jiang, H. Yang, Pore structure characterization of different rank coals using N_2 and CO_2 adsorption and its effect on CH_4 adsorption capacity: A case in Panguan syncline, western Guizhou, China, Energy Fuel. 31 (2017) 6034–6044.

https://doi.org/10.1021/acs.energyfuels.7b00675.

[42] H. Liu, C. Liu, G. Bai, C. Zhu, Study on the effect of chloride ion ingress on the pore structure of the attached mortar of recycled concrete coarse aggregate, Constr. Build. Mater. 263 (2020) 120123. https://doi.org/10.1016/j.conbuildmat.2020.120123.

[43] M. Sammalkorpi, M. Karttunen, M. Haataja, Ionic surfactant aggregates in saline solutions: sodium dodecyl sulfate (SDS) in the presence of excess sodium chloride (NaCl) or calcium chloride ($CaCl_2$), J. Phys. Chem. B, 113 (2009) 5863–5870. https://doi.org/10.1021/jp901228v.

[44] T. Kim, The effects of polyaluminum chloride on the mechanical and microstructural properties of alkali-activated slag cement paste, Cem. Concr. Compos. 96 (2019) 46–54. https://doi.org/10.1016/j.cemconcomp.2018.11.010.

[45] W.A. Hunnicutt, P. Mondal, L.J. Struble, Effect of aluminum substitution in CSH on viscoelastic properties: Stress relaxation nanoindentation, Proceedings of the 1st International Conference on Grand Challenges in Construction Materials, Los Angeles, 2016, 17–18.

[46] L.S. Ho, K. Nakarai, M. Duc, A.L. Kouby, A. Maachi, T. Sasaki, Analysis of strength development in cement-treated soils under different curing conditions through microstructural and chemical investigations, Constr. Build. Mater. 166 (2018) 634–646. https://doi.org/10.1016/j.conbuildmat.2018.01.112.

[47] R. Abousnina, A. Manalo, W. Ferdous, W. Lokuge, B. Benabed, K.S. Al-Jabri, Characteristics, strength development and microstructure of cement mortar containing oil-contaminated sand, Constr. Build. Mater. 252 (2020) 119155. https://doi.org/10.1016/j.conbuildmat.2020.119155.

[48] W. Wongkeo, P. Thongsanitgarn, A. Chaipanich, Compressive strength and drying shrinkage of fly ash-bottom ash-silica fume multi-blended cement mortars, Mater. Design, 36 (2012) 655–662. https://doi.org/10.1016/j.matdes.2011.11.043.

[49] A.R. Estabragh, A. Soltani, A.A. Javadi, Effect of pore water chemistry on the behaviour of a kaolin–bentonite mixture during drying and wetting cycles. Eur. J. Environ. Civil Eng. 24 (2020) 895–914. https://doi.org/10.1080/19648189.2018.1428691.

[50] A.K. Suryavanshi, J.D. Scantlebury, S.B. Lyon, Pore size distribution of OPC & SRPC mortars in presence of chlorides, Cem. Concr. Res. 25 (1995) 980–988. https://doi.org/10.1016/0008-8846(95)00093-R.

[51] G.Y. Koga, P. Comperat, B. Albert, V. Roche, R.P. Nogueira, Effect of endogenous chloride contamination on the electrochemical and hydration responses of reinforced Belite-Ye'elimite-Ferrite (BYF) cement mortars, Cem. Concr. Res. 122 (2019) 212–226. https://doi.org/10.1016/j.cemconres.2019.04.022.